

On the Joint Optimization of Energy Harvesting and Sensing of Piezoelectric Energy Harvesters: Case Study of a Cable-Stayed Bridge

P. Peralta-Braz^a, M. M. Alamdari^a, E. Atroshchenko^{1a}, M. Hassan^b

^a*School of Civil and Environmental Engineering, University of New South Wales, Sydney, Australia*

^b*School of Computer Science and Engineering, University of New South Wales*

Abstract

There is growing evidence that piezoelectric energy harvesters (PEHs) not only generate electricity from vibration sources, but their voltage signals can also be utilized simultaneously to sense various contexts of interest. Little is known, however, about any potential trade-off between its energy harvesting and sensing performances within the design space of the PEH device. Lack of such knowledge prevents optimal design of dual-functional PEH devices that are expected to be used both as a power source and a sensing system. In this paper, using an extensive vibration dataset collected from a real-world cable-stayed bridge, we investigate the simultaneous energy harvesting and vehicle speed sensing performance of PEH devices with varying geometrical shapes. Our results reveal that both energy harvesting efficiency and sensing accuracy depend significantly on the shape of the PEH, and there exist configurations with more favourable harvesting and sensing performances. This finding is expected to open up new opportunities for jointly optimizing energy harvesting and sensing for various types of PEH devices and applications.

Keywords: Piezoelectric Energy Harvester, Simultaneous Energy Harvesting and Sensing, Cable-stayed Bridge, Kirchhoff-Love plate.

1. Introduction

While the primary function of piezoelectric energy harvesters (PEHs) is to produce electricity from various vibration sources, there is a growing interest to use the same device as a sensor to detect various environmental contexts. For example, researchers have recently demonstrated that attaching a PEH to a wearable device can not only generate electricity from human activities, but the generated electrical signal can also be directly used as a signature to characterise the activity, i.e., running, walking, jumping [1, 2, 3]. Similarly, attaching the PEH device under a vibrating bridge not only generates electricity from the bridge vibrations, the generated voltage responses can be used to detect events of interest such as detecting times of vehicle's entry and exist to the bridge [4], identifying train passages [5] or even detecting bridge damages [6]. A key benefit of using a PEH as a sensor is that it eliminates the powering requirement of a separate dedicated sensor, such as an accelerometer or strain gauge, thus advancing the possibility of realizing completely self-powered wireless Internet of Things sensors [7].

For a PEH device to act as an effective sensor, it has to be designed with the dual purpose of achieving efficient energy harvesting as well as high sensing accuracy. Although, significant progress has been made in designing efficient PEH from the energy harvesting points of view [8, 9, 10], little

¹Corresponding author

is known about the impact of PEH design parameters, such as its geometrical shapes on its sensing performance. The intent of this work is to explore PEH design spaces to understand the impact of design configurations on both energy harvesting as well as sensing accuracy. The knowledge gained from this exercise allows dual-function PEHs' design that are favourable for both energy harvesting and sensing. To realize our goal, we evaluated both energy harvesting efficiency and vehicle speed sensing accuracy of six different shapes of a cantilever-type PEH fed by an extensive vibration dataset collected from a large-scale operating cable-stayed bridge. Our results reveal that both energy harvesting efficiency and sensing accuracy depend significantly on the shape of the PEH, and there exist configurations with more favourable harvesting and sensing performances. This finding indicates potential opportunities for jointly optimizing energy harvesting and sensing for various types of PEH devices and applications.

The contributions of this paper can be summarised as follows:

1. Using real field datasets from an operating cable-stayed bridge, we make the first attempt in exploring the impact of PEH geometry on both energy harvesting and sensing accuracy in the context of a vehicle speed estimation.
2. We present a deep learning framework to evaluate the vehicle speed sensing performance of PEHs with various designs.
3. We report evidences, for the first time, that there are design trade-offs between energy harvesting and sensing, i.e., PEH designs that provide peak energy, cannot necessarily provide peak sensing accuracy. This finding opens opportunities for more investigations into joint optimization of energy harvesting and sensing for PEH.

The rest of the paper is organised as follows. The cable-stayed bridge studied in this work is presented in Section 2. In Section 3, the theoretical framework of the PEH model is explained. Next, the deep learning framework to infer the vehicle speed on bridges using PEHs is presented in Section 4. Finally, evaluation results are presented in Section 5 before concluding the paper in Section 6.

2. Case Study: A Cable-Stayed Bridge

The study will carry out on a cable-stayed bridge located over the Great Western Highway in the state of New South Wales (NSW), Australia (Figure 1). The bridge has one traffic lane and one pedestrian lane with a maximum loading capacity of 30 tons. The bridge's deck is supported by four longitudinal girders, which are internally attached by seven transverse girders, see Figure 2. The bridge has an array of sensors installed under the deck, including accelerometers and strain gauges. For the purpose of this study one accelerometer sensor (A1), and two pairs of strain gauge sensors (SS1:SS4), as shown in Figure 2, are adopted. These sensors are continuously measuring the dynamic response of the bridge at a sampling frequency of 600 Hz. The collected data from the accelerometer A1 will be employed to estimate the potential harvested energy from the passing traffic, and further infer the corresponding traffic speed. Additionally, the two pairs of strain gauge sensors are used to estimate the ground-truth velocity and consequently label samples in the training and validation database used for the Neural Network (NN) model. The vehicle speed is independently estimated from strain gauge sensors SS1-SS2 and SS3-SS4. As the sensors are installed at known distances under the bridge span, the time difference that one vehicle's axle travels from one sensor to another allows for estimating the vehicles' speed (refer [11] for more details). Although, only one pair of sensors can be used for speed estimation, it was decided to use two independent pairs to improve the reliability of the estimation by averaging.



Figure 1: Studied cable-stayed bridge located in the state of NSW, Australia [12].

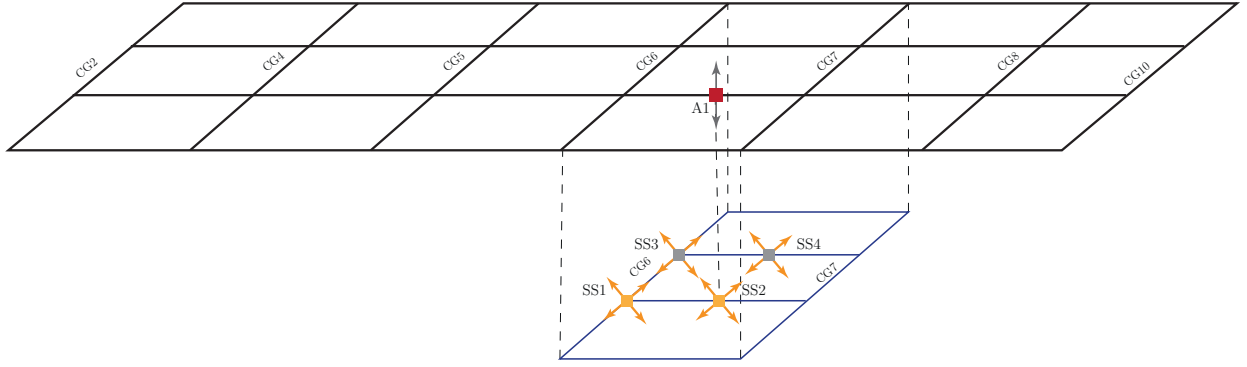


Figure 2: Illustration of the sensors under the deck.

3. Cantilever-Type Piezoelectric Plate Model

There are several models to estimate the dynamic response of a cantilever-type piezoelectric harvester in the literature. One of them being through Iso-Geometric Analysis (IGA) framework for a PEH [9], which stands out due to its higher accuracy reached in reduced computational time. This is the reason why this model is selected for the present work. Figure 3 presents a schematic of the piezoelectric energy harvester adopted in this study.

The model formulation is based on the Kirchhoff-Love plate theory and Hamilton's generalized principle for electro-mechanical bodies. The model is solved numerically using the IGA method, where B-Splines N_I describe the device's domain, and the deflection field \mathbf{w} is approximated using the same basis functions N_I . The framework was presented in [9], where the relative deflection solution \mathbf{w} can be approximated by a truncated expansion of the first K mode shape vectors $\mathbf{w}_o = \Phi_o \boldsymbol{\eta}$. Here, $\Phi_o \in \mathbf{R}^{N \times K}$ is the matrix which contains the K first mode shape vectors ϕ_i and $\boldsymbol{\eta} \in \mathbf{R}^{K \times 1}$ denotes the modal coordinates. Therefore, the procedure leads to a coupled system of differential equations of the form,

$$\ddot{\boldsymbol{\eta}} + \mathbf{c}_o \dot{\boldsymbol{\eta}} + \mathbf{k}_o \boldsymbol{\eta} - \boldsymbol{\theta}_o v = \mathbf{f}_o a_b(t) \quad (1)$$

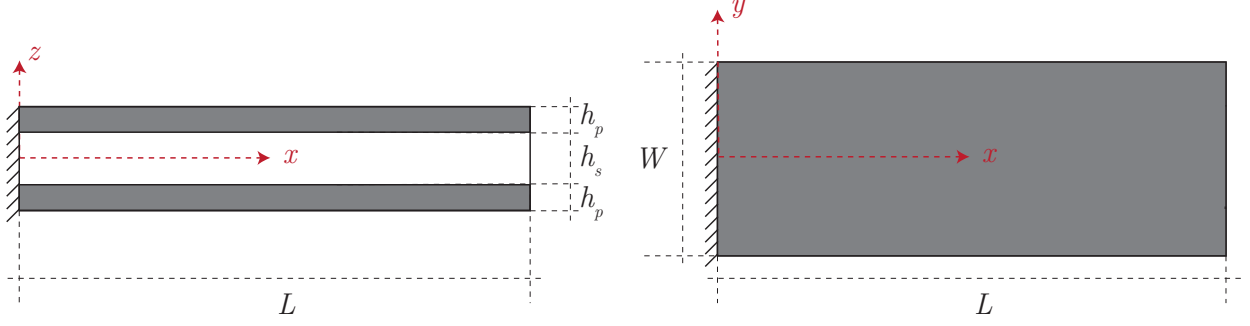


Figure 3: Illustration of the piezoelectric energy harvester, modeled as a cantilever plate, consisting of two piezoelectric layers and one substructure layer.

$$C_p \dot{v}(t) + \frac{v(t)}{R_l} + \Theta^T \Phi_o \dot{\eta} = 0 \quad (2)$$

where the equation (1) corresponds to the reduced mechanical equation of motion with electrical coupling, while the equation (2) corresponds to the reduced electrical circuit equation with mechanical coupling. Here, $\mathbf{k}_o \in \mathbf{R}^{K \times K}$ is the reduced stiffness matrix, $\mathbf{c}_o \in \mathbf{R}^{N \times N}$ is the reduced mechanical damping matrix, $\mathbf{f}_o \in \mathbf{R}^{K \times 1}$ is the mechanical forces vector, $\Theta \in \mathbf{R}^{N \times 1}$ is the reduced electro-mechanical coupling vector, $\theta_o \in \mathbf{R}^{K \times 1}$ is the electro-mechanical coupling vector; C_p is the capacitance and R_l is the external electric resistance.

It is possible to define the Frequency Response Function (FRF) that relates the amplitudes of the output voltage V_o and the excitation acceleration A_b for a specific frequency ω from the equations (1) and (2), considering that the base acceleration and response voltage are harmonic signals of the form $a_b(t) = A_b e^{i\omega t}$ and $v(t) = V_o e^{i\omega t}$ (where $i = \sqrt{-1}$),

$$H_v(\omega) = \frac{V_o(\omega)}{A_b} = i\omega \left(\frac{1}{R_l} + i\omega C_p \right)^{-1} \Theta^T \Phi_o \left(-\omega^2 \mathbf{I}_o + j\omega \mathbf{c}_o + \mathbf{k}_o + i\omega \left(\frac{1}{R_l} + i\omega C_p \right)^{-1} \theta_o \Theta^T \Phi_o \right)^{-1} \mathbf{f}_o \quad (3)$$

From the differential equations presented in equations (1) and (2), it is also possible to estimate the voltage signal in time when the piezoelectric device is subjected to an arbitrary base acceleration of a_b , which particularly in this study it represents the acceleration measured from a vibrating bridge as a result of passing traffic. The system of differential equations can be represented in its state-space representation,

$$\dot{\mathbf{Z}} = \mathbf{A} \cdot \mathbf{Z} + \mathbf{b} \cdot a_b(t) \quad (4)$$

where,

$$\mathbf{Z} = \begin{bmatrix} \eta \\ \dot{\eta} \\ v \end{bmatrix}, \mathbf{A} = \begin{bmatrix} 0 & 1 & 0 \\ -\mathbf{k}_o & -\mathbf{c}_o & \theta_o \\ 0 & -\frac{\Theta^T \Phi_o}{C_p} & -\frac{1}{C_p R_l} \end{bmatrix}, \mathbf{b} = \begin{bmatrix} 0 \\ \mathbf{f}_o \\ 0 \end{bmatrix}$$

Simulink ode45 solver is proposed to solve this equation, from which it is possible to estimate the generated voltage time history $v(t)$. Note that once $v(t)$ is estimated, the electrical energy, E can be achieved according to the following equation where $P(t)$ is the electrical power,

$$E = \int_{t_1}^{t_2} P(t) dt = \int_{t_1}^{t_2} \frac{v^2(t)}{R_l} dt \quad (5)$$

Therefore, based on the framework detailed in this section, one can obtain the voltage generated by a PEH in response to the passage of a vehicle over the bridge. In the next section, a procedure to obtain the speed of the moving vehicle from the acquired voltage signal $v(t)$ is presented.

4. Deep Learning Approach

In this section a deep-learning-based framework is presented to infer a passing vehicle's speed from the generated voltage signal by a PEH installed under the bridge. To address this problem, we extend and validate the methodology proposed by Zhou et al. [13].

As indicated in Figure 4, two main parts can be identified in this framework. In the sample generation part, the first step is to extract the time window corresponding to a passing vehicle, e.g., an event, and consequently obtain the corresponding acceleration and strain response of the sensors attached to the bridge (see Figure 2). Next, the voltage response is estimated from the acceleration signal using the numerical framework presented in section 3. Meanwhile, the vehicle speed labels are estimated from the strain signals following the procedure explained in [11]. Further, the raw time signals of the voltage is post-processed using the time-frequency analysis to extract traffic-dependant information. Following the recommendation in [13], Continuous Wavelet Transformation (CWT) is employed using Morlet Wavelet, which shows promise in the context of our problem.

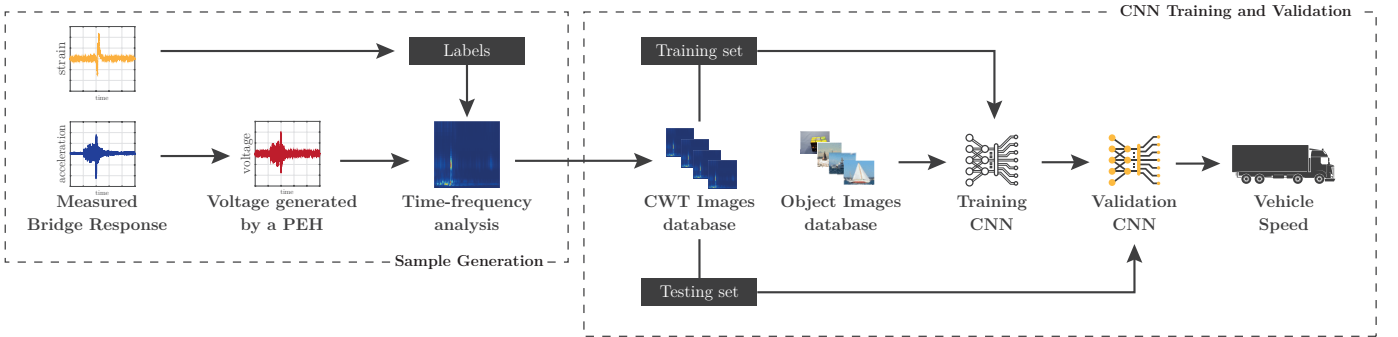


Figure 4: Overview of deep learning framework comprised of two main parts: sample generation, and Convolutional Neural Network (CNN) training and validation.

The second part of the methodology is the Convolutional Neural Network (CNN) for training and testing. To this aim, the first step is to build a database following the procedure of the sample generation. The data is divided into two sets of training and testing. The selected architecture for CNN in this paper is AlexNet [14] due to its excellent ability to extract local and multilevel features in different applications, and its successful implementation in vehicle classification in earlier work [13]. AlexNet consists of eight layers, where the first five are convolutional layers, (some of them followed by max-pooling layers), and the last three are fully connected (FC) layers, as shown in Figure 5. AlexNet requires a vast database for its training; for this reason, in [13] a Transfer Learning method [15, 16] was proposed to reduce the size of the required databases. In this method, an alternative data is used to train lower-level layers, which are responsible for extracting the generic features of the input data. While, the real data is used to train the last layers, which carry out the classification task. Finally, the trained model accuracy is estimated using the validation dataset.

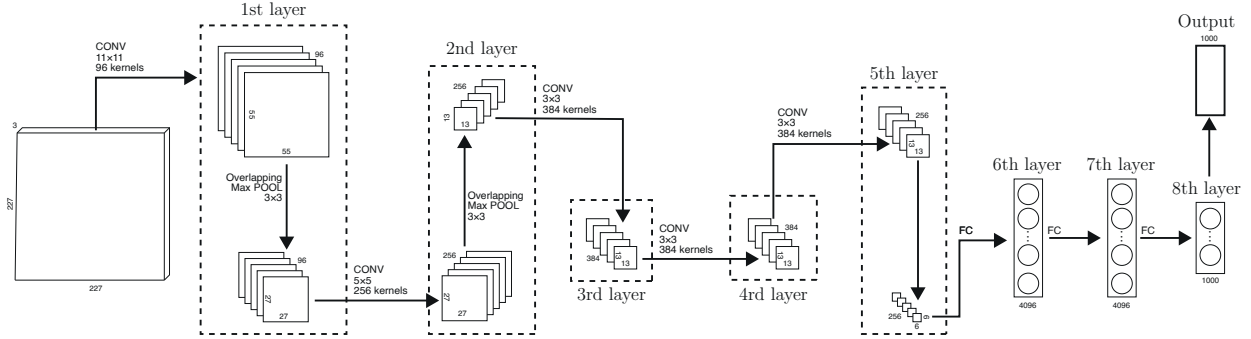


Figure 5: The architecture of the adopted CNN method in this paper using AlexNet.

Table 1: Definition of the classification labels

Label	Definition	# Samples
30 km/h	speed \in [30, 38] km/h	649
40 km/h	speed \in [42, 48] km/h	490
50 km/h	speed \in [50, 60] km/h	126

5. Results and Discussions

In this section, the methodology proposed in section 4 is extensively investigated. A benchmark case is first presented, where the acceleration data are directly used for speed estimation, without transferring into the corresponding voltage generated by a PEH. Following that, a study case is presented where the method is applied considering six different configurations of PEHs, which only differ in their length L . Unlike the benchmark case, in this case study the generated voltage output from each PEH device is adopted for training and testing and consequently estimating the speed of the passing traffic. The studied PEHs are compared in terms of energy harvesting and sensing accuracy. In each implementation, the database is divided randomly into two sets for training and validation processes, containing 70% and 30% of the data, respectively. Also, the training-testing process is performed multiple times to reduce the stochastic factors. For the sake of this study, a total of 1265 samples are considered, which are classified into three different labels, as presented in Table 1.

5.1. Benchmark Case

In this section, a case study is carried out which serves as a benchmark for the subsequent cases. The results obtained from this case study are compared with counterpart results reported in the literature performed on an experimental setup in a laboratory. As mentioned, in this case the use of PEH is not considered, and the acceleration data is directly used, i.e., the transformation into voltage signal is not considered.

The acceleration response windows is taken to be 25 second. This selection is based on the span length of the bridge under investigation, and the min-max speed range on this bridge, so not to miss any passing traffic event. To obtain each event from the dataset, (please note that the extracted acceleration from the bridge is the continuous response measured at 600Hz, and further post-processing is required to extract the events as a result of passing traffic), first local peak in the response is identified, and then a time window starting 10 second before the peak and ends 15 second after the peak is considered, as shown Figure 6a.

Further, time-frequency analysis using CWT is performed to obtain two-dimensional time-frequency images. For the sake of consistency, all images are produced considering a time limit of [5-25] second and a frequency limit of [0-200] Hz, as shown Figure 6b.

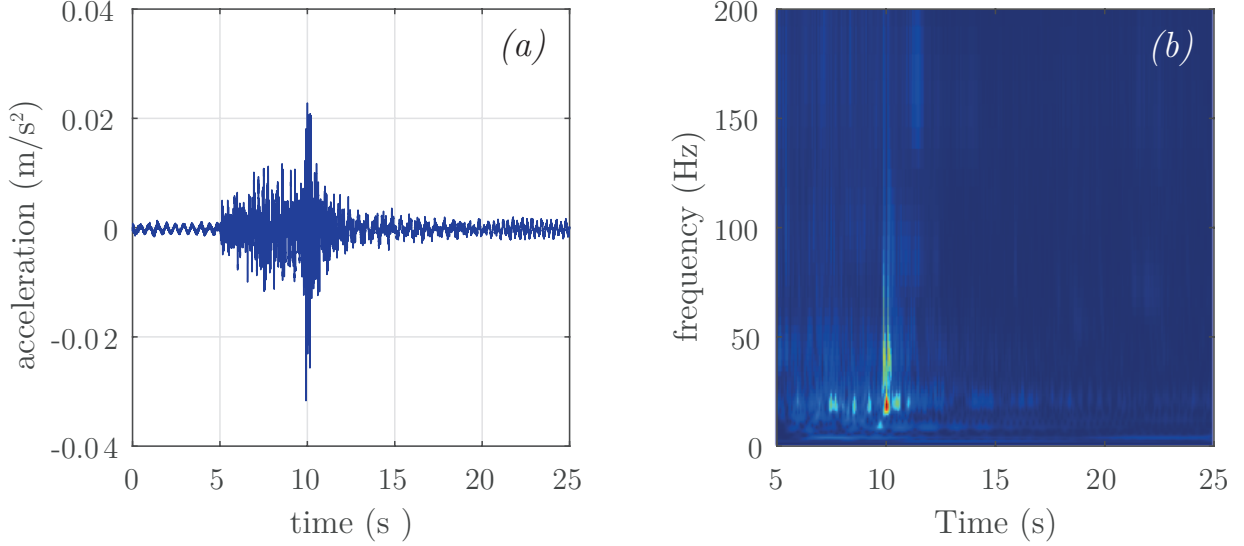


Figure 6: (a) An arbitrary acceleration time window induced on the bridge by a passing vehicle. (b) The corresponding CWT image.

The training process is carried out 5 times, to reduce the impact of random factors, where, each time, 70% of the data is randomly extracted for training. In Figures 7a and 7b, the accuracy and loss curves are, respectively, presented. From these figures, the loss continuously decreases across the epochs, and the accuracy tends to converge 1 at about 50 epochs. Furthermore, Figure 7c presents the accuracy obtained from the validation dataset. The average accuracy of the five validation sets is 0.932, which is in agreement with the accuracy reported in [13] between 0.929 - 0.988. Additionally, the confusion matrix of validation set 5 is presented in Figure 7d.

5.2. Study Case

In this section, the full framework proposed in section 4 is employed for six different PEH designs. The materials of the devices are PZT5A and bronze [9], where the remaining parameters are tabulated in Table 2. The devices share the same geometric parameters, except for the length L . In particular, the device's lengths L are 5, 10, 15, 20, 25, 30 cm. Other important considerations for the PEH model is that the external electrical resistance is considered to be $R_l = 100$ ohm, and the damping coefficients are considered to be $\alpha = 14.65$ rad/s and $\beta = 10^{-5}$ rad/s [9].

Table 2: Geometric parameters of the studied PEH devices.

Width W	50	mm
Piezoelectric Thickness h_p	0.25	mm
Substructure Thickness h_s	0.50	mm

Figure 8 presents the FRFs of the six studied devices. Note the effect of varying the length L among devices on the dynamic response, where the resonant frequencies vary as a function of the

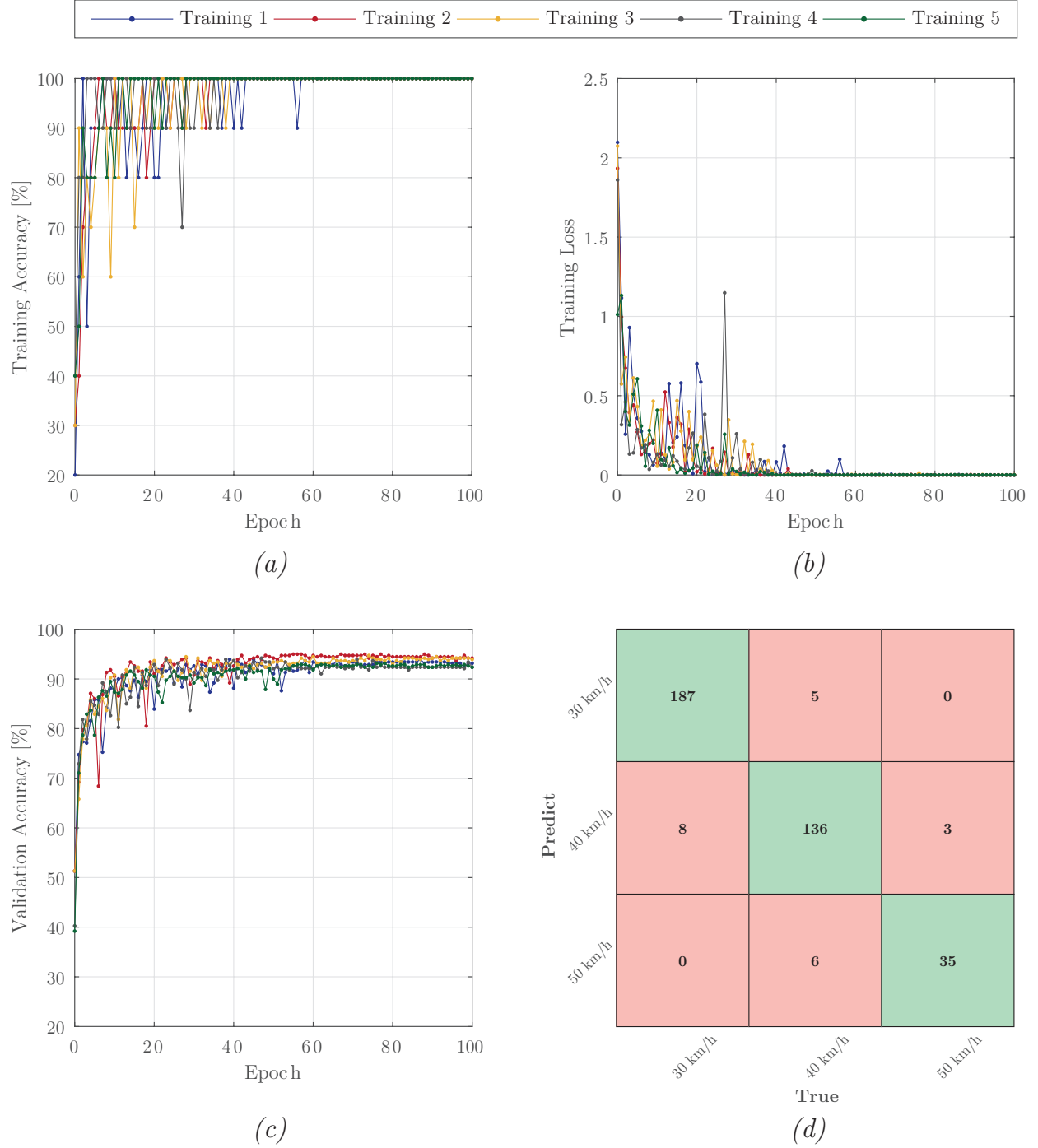


Figure 7: (a) Accuracy in the training process. (b) Loss in the training process. (c) Accuracy on the validation data across the training process. (d) Confusion matrix in the validation set 5.

length L . Furthermore, as the device length L increases, the device tends to be more flexible with more modes appearing in the range of 0 - 200 Hz.

Similar to the benchmark case, the neural network is trained five times for each case. Thus, it is possible to estimate the average accuracy with greater reliability. Figure 9 presents the mean value and error bars for the six devices considered. The device's accuracy varies, reaching the highest value for the device with a length of 25 cm, which interestingly this accuracy is higher than that obtained

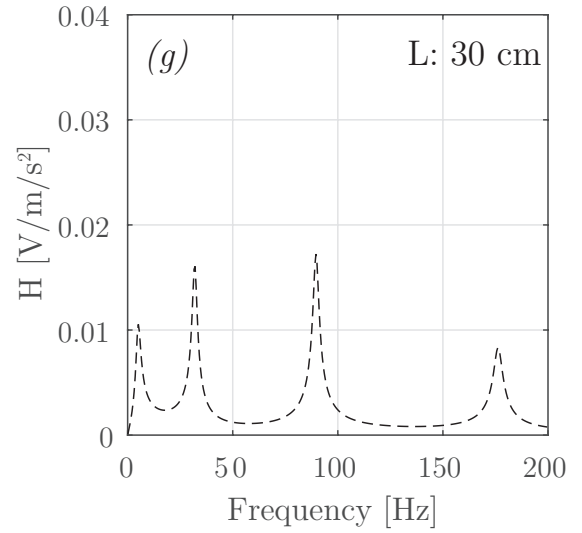
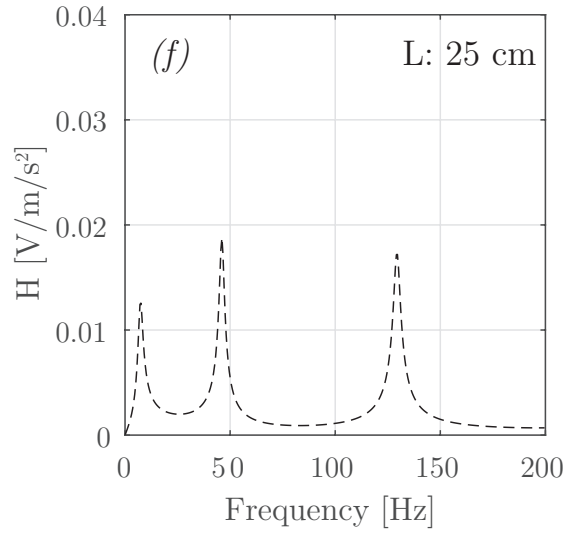
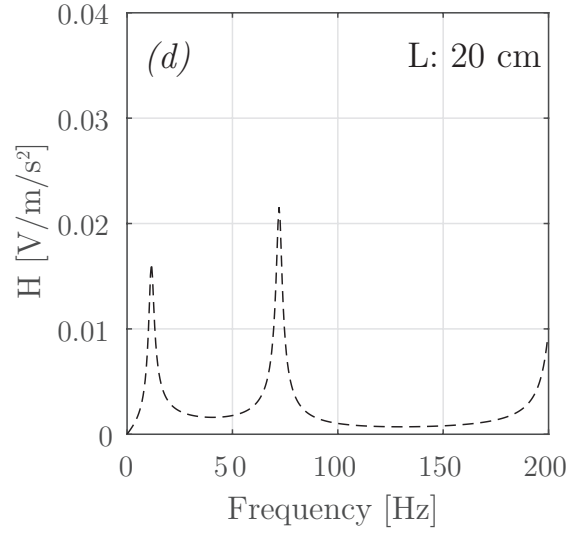
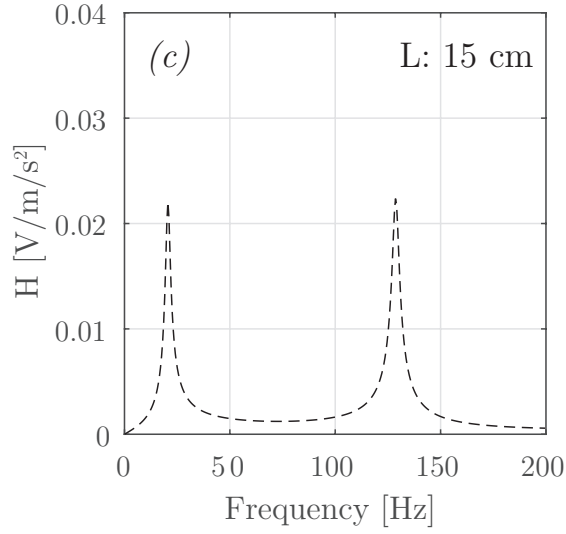
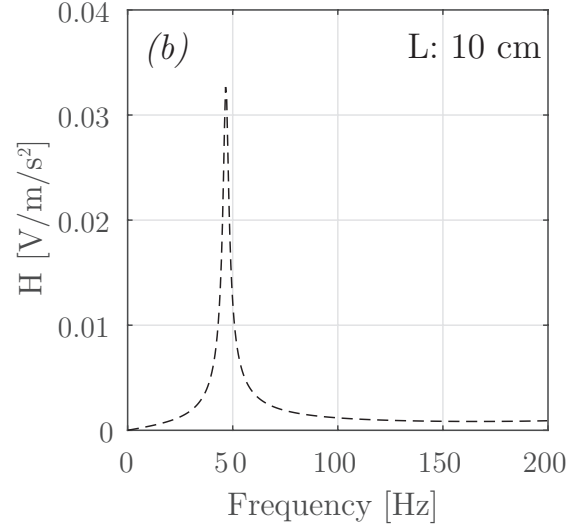
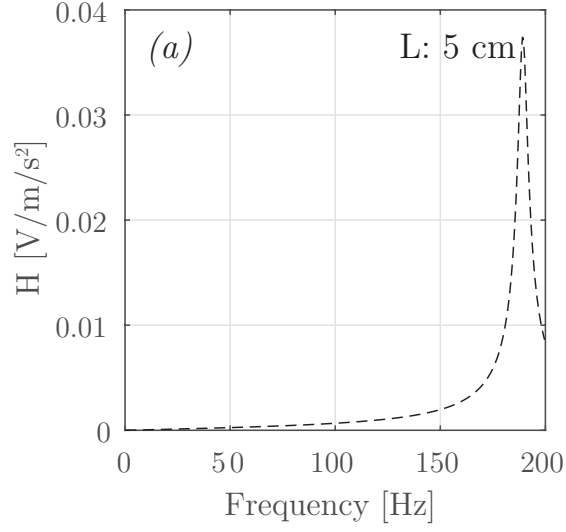


Figure 8: Frequency response function of the six devices studied with a length of (a) 5 cm (b) 10 cm (c) 15 cm (d) 20 cm (f) 25 cm (g) 30 cm.

from the benchmark case.

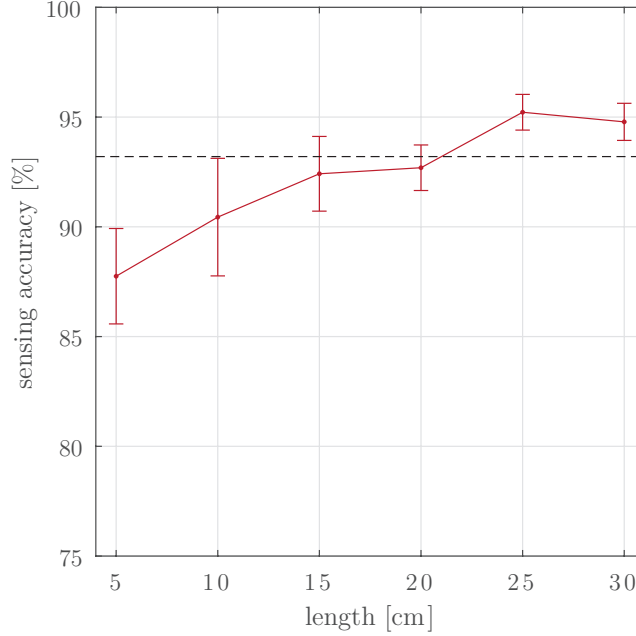


Figure 9: Bar plot of accuracy from five different training processes for the six devices studied.

To interpret these results, it is necessary to consider that CNN extracts information from the time-frequency images. Figure 10 presents the CWT images of the generated voltage from the reference acceleration window, previously presented in Figure 6. These images are obtained from the six PEH devices considered. The pink dashed lines represent the resonance frequencies of each device identified from the FRFs, presented earlier in Figure 8. As shown in Figure 10, the highest values of wavelet coefficients, and consequently the most informative parts of these images are centred at frequencies close to the resonance frequencies of each PEH device. Further, since devices with different length associate with different resonance frequencies, the amount of information they provide will differ, which consequently leads to different sensing performance in terms of correctly labelling the class of speed. Next, A question arises on how the sensing accuracy and power generation are correlated. This issue will be addressed in the next section.

5.3. Energy Harvesting Performance

In this section the electrical energy harvested from each of the six PEH devices is studied to establish a correlation between the optimal design in terms of sensing and energy harvesting performances. Five 12-hour continuous time windows of acceleration response, between 8 am and 9 pm, are used to estimate the six candidates' average energy generated from five separate days. The energy is estimated using equation (5).

Figure 11a presents the harvested energy, and the corresponding variation from the five different days considered. From this figure, it is evident that the highest energy generation corresponds to the device with a length of 15 cm. This is explained by analysing Figure 12, where the acceleration frequency spectrum of one 12-hour acceleration window from the bridge is compared with the FRFs of the six PEH devices. It can be seen that the resonance frequency of the optimal device with a length of 15 cm coincides well with dominant parts of the base excitation with frequencies around 21

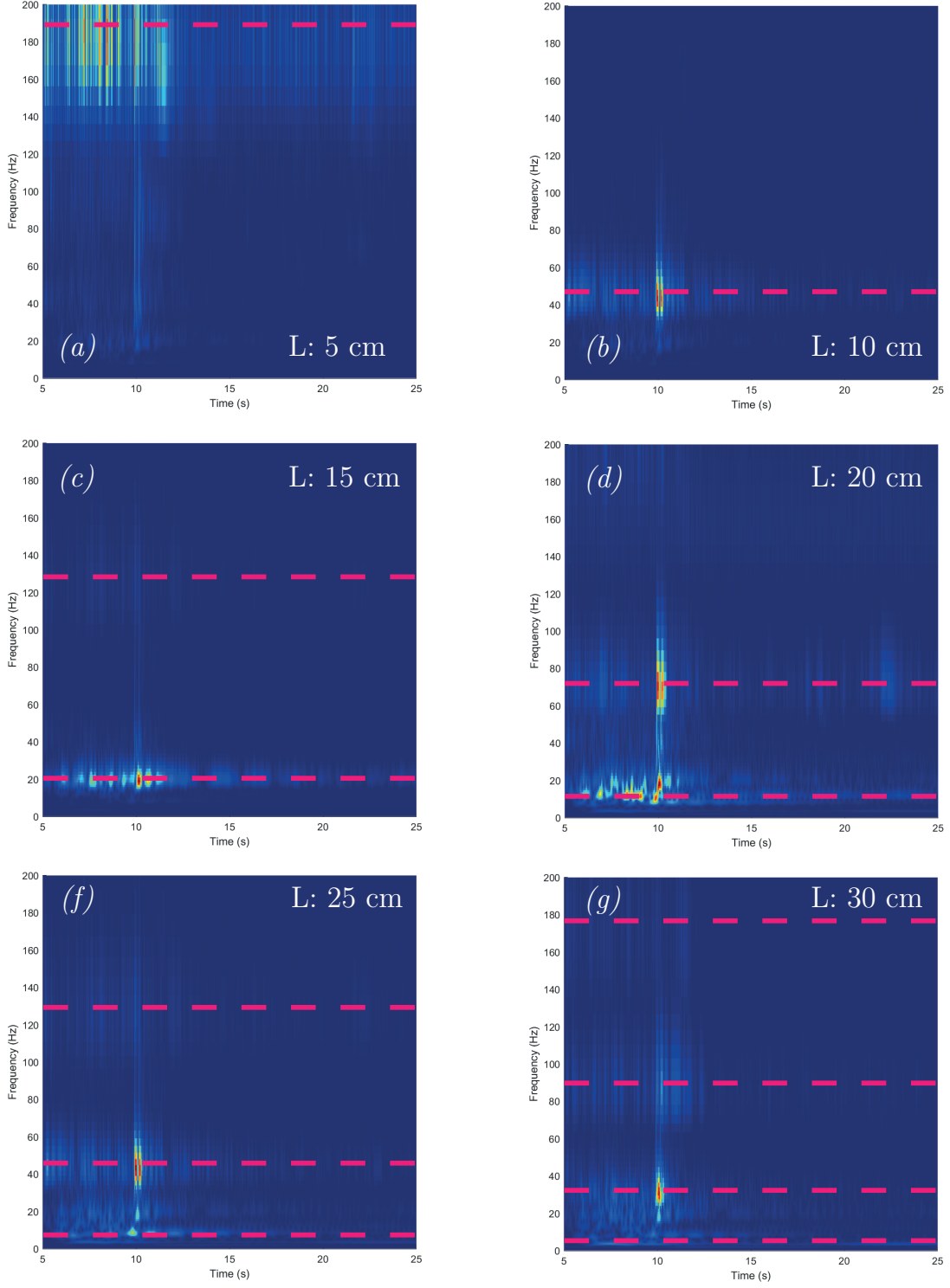


Figure 10: Time-frequency image of the generated voltage (from the reference acceleration time window) obtained from the six PEH devices studied with a length of (a) 5 cm (b) 10 cm (c) 15 cm (d) 20 cm (e) 25 cm (f) 30 cm.

Hz, which results in a higher energy generation compared to the other geometries.

Further, Figure 11b compares the sensing performance of the six PEH devices with the corresponding energy harvesting performance. From this figure, it is implied that there is no correlation between

the optimal geometries in terms of sensing performance and energy harvesting performance. This observation opens up a great opportunity for joint optimisation of sensing/harvesting performances of PEH devices.

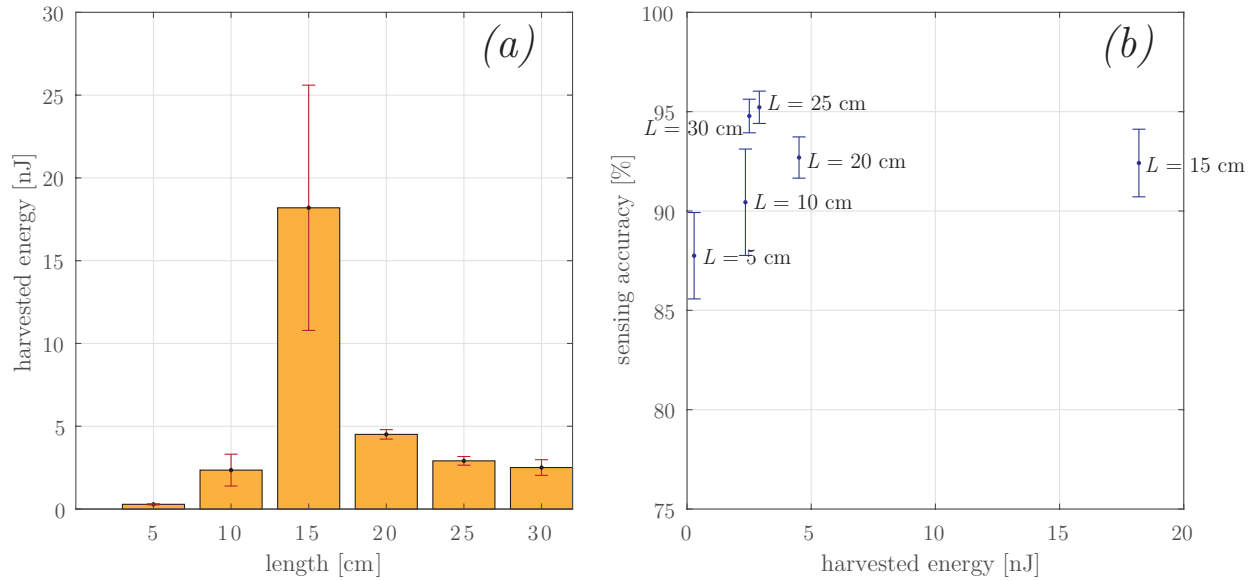


Figure 11: (a) Energy harvested from the six studied PEH devices obtained from five separate days. (b) Comparison of the energy harvesting performance and the sensing accuracy performance of the six PEH devices considered.

6. Conclusions

Using real vibration datasets from a cable-stayed bridge, we studied the performance of six PEH geometries in terms of both energy harvesting and sensing to correctly label the travelling speed of vehicles passing over the bridge. We found that there is no clear correlation between energy harvesting and sensing performance for a PEH. In other words, an optimum harvester may not necessarily act as an optimum sensor. This finding motivates future works to more rigorously design and study a joint optimization of dual-function PEH devices that are expected to provide both energy harvesting and sensing functionality for future self-powered IoT sensors.

Acknowledgements

The authors wish to thank CSIRO's Digital Productivity business unit, Data61 for providing the research data. The instrumentation and the field tests of this bridge have been planned and conducted by researchers at Data61 in collaboration with academics at University of New South Wales (UNSW). The authors wish also thank the Faculty of Engineering at UNSW for provision of selective seed funding under the GROW scheme.

References

- [1] S. Khalifa, G. Lan, M. Hassan, A. Seneviratne, S. K. Das, Harke: Human activity recognition from kinetic energy harvesting data in wearable devices, *IEEE Transactions on Mobile Computing* 17 (2018) 1353–1368.

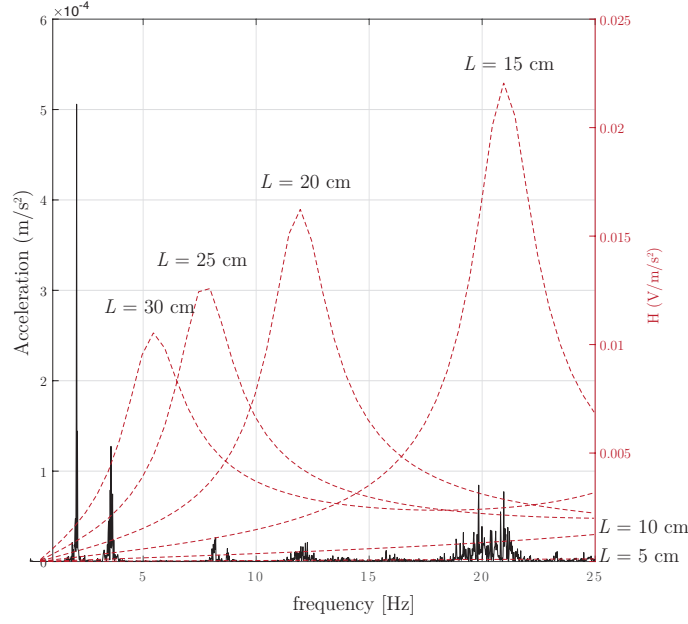


Figure 12: Acceleration frequency spectrum of one 12-hour acceleration window (shown in black), and the FRFs of the six PEH devices considered (shown in red).

- [2] D. Ma, G. Lan, W. Xu, M. Hassan, W. Hu, Sehs: Simultaneous energy harvesting and sensing using piezoelectric energy harvester, in: 2018 IEEE/ACM Third International Conference on Internet-of-Things Design and Implementation (IoTDI), IEEE, pp. 201–212.
- [3] D. Ma, G. Lan, W. Xu, M. Hassan, W. Hu, Simultaneous energy harvesting and gait recognition using piezoelectric energy harvester, IEEE Transactions on Mobile Computing 21 (2022) 2198–2209.
- [4] Z. Zhang, H. Xiang, Z. Shi, J. Zhan, Experimental investigation on piezoelectric energy harvesting from vehicle-bridge coupling vibration, Energy Conversion and Management 163 (2018) 169–179.
- [5] P. Cahill, B. Hazra, R. Karoumi, A. Mathewson, V. Pakrashi, Vibration energy harvesting based monitoring of an operational bridge undergoing forced vibration and train passage, Mechanical Systems and Signal Processing 106 (2018) 265–283.
- [6] P. C. Fitzgerald, A. Malekjafarian, B. Bhowmik, L. J. Prendergast, P. Cahill, C.-W. Kim, B. Hazra, V. Pakrashi, E. J. O'Brien, Scour damage detection and structural health monitoring of a laboratory-scaled bridge using a vibration energy harvesting device, Sensors 19 (2019) 2572.
- [7] D. Ma, G. Lan, M. Hassan, W. Hu, S. K. Das, Sensing, computing, and communications for energy harvesting iots: A survey, IEEE Communications Surveys and Tutorials 22 (2020) 1222–1250.
- [8] A. C. Hurtado, P. Peralta, R. Ruiz, M. M. Alamdari, E. Atroshchenko, Shape optimization of piezoelectric energy harvesters of variable thickness, Journal of Sound and Vibration 517 (2022) 116503.
- [9] P. Peralta, R. Ruiz, S. Natarajan, E. Atroshchenko, Parametric study and shape optimization of piezoelectric energy harvesters by isogeometric analysis and kriging metamodeling, Journal of Sound and Vibration 484 (2020) 115521.

- [10] G. Lee, D. Lee, J. Park, Y. Jang, M. Kim, J. Rho, Piezoelectric energy harvesting using mechanical metamaterials and phononic crystals, *Communications Physics* 5 (2022) 1–16.
- [11] H. Kalhori, M. M. Alamdari, X. Zhu, B. Samali, S. Mustapha, Non-intrusive schemes for speed and axle identification in bridge-weigh-in-motion systems, *Measurement Science and Technology* 28 (2017) 025102.
- [12] K. Kildashti, M. M. Alamdari, C. Kim, W. Gao, B. Samali, Drive-by-bridge inspection for damage identification in a cable-stayed bridge: Numerical investigations, *Engineering structures* 223 (2020) 110891.
- [13] Y. Zhou, Y. Pei, S. Zhou, Y. Zhao, J. Hu, W. Yi, Novel methodology for identifying the weight of moving vehicles on bridges using structural response pattern extraction and deep learning algorithms, *Measurement* 168 (2021) 108384.
- [14] A. Krizhevsky, I. Sutskever, G. E. Hinton, Imagenet classification with deep convolutional neural networks, *Advances in neural information processing systems* 25 (2012).
- [15] S. J. Pan, Q. Yang, A survey on transfer learning, *IEEE Transactions on knowledge and data engineering* 22 (2009) 1345–1359.
- [16] M. Oquab, L. Bottou, I. Laptev, J. Sivic, Learning and transferring mid-level image representations using convolutional neural networks, in: *Proceedings of the IEEE conference on computer vision and pattern recognition*, pp. 1717–1724.